ACS APPLIED MATERIALS & INTERFACES

Research Article

www.acsami.org

Superhydrophobic Surface-Enhanced Raman Scattering Platform Fabricated by Assembly of Ag Nanocubes for Trace Molecular Sensing

Hiang Kwee Lee,[†] Yih Hong Lee,[†] Qi Zhang,[†] In Yee Phang,[‡] Joel Ming Rui Tan,[†] Yan Cui,[†] and Xing Yi Ling*,[†]

[†]Division of Chemistry and Biological Chemistry, School of Physical and Mathematical Sciences, Nanyang Technological University, Singapore 637371

[‡]Institute of Materials Research and Engineering, A*STAR (Agency for Science, Technology and Research), 3 Research Link, Singapore 117602

Supporting Information

ABSTRACT: An analytical platform suitable for trace detection using a small volume of analyte is pertinent to the field of toxin detection and criminology. Plasmonic nanostructures provide surface-enhanced Raman scattering (SERS) that can potentially achieve trace toxins and/or molecules detection. However, the detection of highly diluted, small volume samples remains a challenge. Here, we fabricate a superhydrophobic SERS platform by assembling Ag nanocubes that support strong surface plasmon and chemical functionalization for trace detection with sample volume of just 1 μL. Our strategy integrates the intense electromagnetic field confinement generated by Ag nanocubes with a superhydrophobic surface capable of analyte concentration to lower the molecular detection limit. Single crystalline Ag nanocubes are assembled using the Langmuir-Blodgett technique to create surface roughness. To create a stable superhydrophobic SERS platform, an additional 25 nm Ag coating is evaporated over the Ag nanocubes to "weld" the Ag nanocubes onto the substrate followed by chemical functionalization with perfluorodecanethiol. The resulting substrate has an advancing contact angle of 169° ± 5°. Our superhydrophobic platform confines analyte molecules within a small area and prevents the random spreading of molecules. An analyte concentrating factor of 14-fold is attained, as compared to a hydrophilic surface. Consequently, the detection limit of our superhydrophobic SERS substrate reaches 10^{-16} M (100 aM) for rhodamine 6G using 1 μL analyte solutions. An analytical SERS enhancement factor of 10^{11} is achieved. Our protocol is a general method that provides a simple, cost-effective approach to develop a stable and uniform superhydrophobic SERS platform for trace molecular sensing.

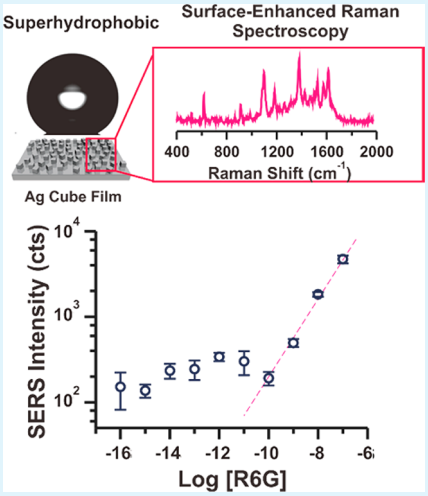

KEYWORDS: *superhydrophobic, surface-enhanced Raman spectroscopy, plasmonic, silver nanocube, trace molecular detection*

INTRODUCTION

Fabricating an analytical platform capable of sensing highly diluted, small volume analyte is essential in trace toxins and/or molecules detection, especially when sample availability is scarce and/or safety issues may arise from the handling of large sample volumes.[1−3] Examples of toxins in which exposure to large volumes should be minimized are arsenic and hexavalent chromium, while scarce sample availability is typical in crime scene or biological examination.[4] Surface-enhanced Raman scattering (SERS) is suitable for this application because of its high sensitivity that can provide fingerprint information.[5,6] The ultrasensitivity of SERS is primarily due to the enhanced electromagnetic field experienced by analyte molecules in the vicinity of metal nanostructures. The coherent oscillations of conduction band electrons give rise to localized surface plasmon resonances in metal nanostructures, which can concentrate light into subwavelength volumes and increase the local electromagnetic field by a factor as high as E^4.[7] Studies have shown that local electromagnetic fields are most intense along the sharp edges/vertices of plasmonic nanostructures as well as in the gap region between adjacent plasmonic nanostructures.[8−12]

Despite the superior sensitivity of SERS, highly diluted, small volume analyte detection remains a challenge. This is due to the random spreading of analyte molecules over SERS substrates, commonly based on hydrophilic Au and/or Ag nanomaterials, which limits the SERS detection sensitivity.[13−15] Superhydrophobicity overcomes the random spreading issue by concentrating analyte molecules into a small area (or volume) arising from the small superhydrophobic substrate−water

Received: August 28, 2013
Accepted: October 17, 2013
Published: October 17, 2013

 © 2013 American Chemical Society

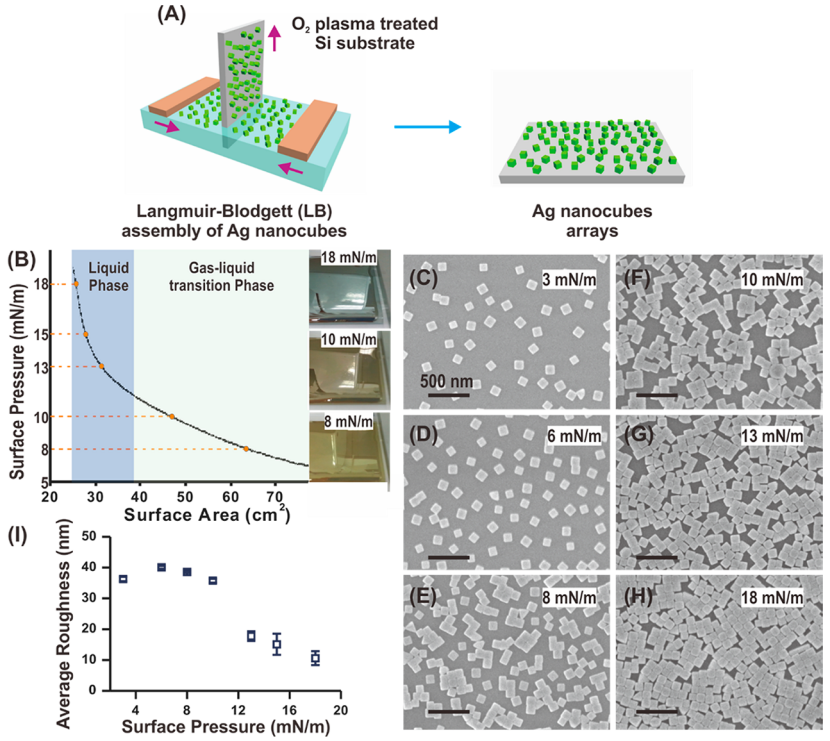

Figure 1. Application of Langmuir-Blodgett to create assembled Ag nanocube array of varying roughness. (A) Schematic of Ag nanocubes (green) array prepared by Langmuir-Blodgett (LB) deposition on an O_2-plasma treated silicon substrate. (B) Isotherm of the Langmuir-Blodgett setup which relates surface pressure (Π) as a function of surface area. Digital pictures beside the plot show the effect of increasing compactness of the monolayer on the liquid−air interface, from an initial liquid−gas transition phase (translucent green, dispersed state) to a liquid phase (metallic silver, compact state). (C−H) refer to SEM images of Ag nanocube array at surface pressures of 3, 6, 8, 10, 13, and 18 mN m^{-1}, respectively, before Ag coating. (I) Correlation of average surface roughness to surface pressure of Langmuir-Blodgett.

interface, thereby further improving SERS detection sensitivity. Superhydrophobic surfaces with hierarchical micro- and nanoscale surface roughness and hydrophobic chemical functionality, such as lotus-[16,17] and rose-petal-like[18,19] surfaces, possess superior anti-wetting ability with a water contact angle greater than 150°.[20−25] It has been shown that a 2-fold decrease in spot diameter on a superhydrophobic SERS substrate leads to a corresponding 4-fold enhancement in SERS intensity, as compared to a hydrophilic SERS substrate.[26] Current superhydrophobic SERS substrate fabrications generally involve two steps: creating a nonmetallic superhydrophobic surface, followed by the deposition of metal film and/or nanoparticles to impart plasmonic properties to the superhydrophobic surface.[27−30] For instance, superhydrophobic nanopatterns fabricated by electron beam and photo-lithography decorated with electroless-deposited Ag films can achieve attomolar (10^{-18} M) rhodamine 6G SERS sensing using a 20 μL analyte solution.[27] However, the equipment and fabrication procedures involved are expensive and sophisticated. Quality (Q-) factor in plasmon resonance, an indication of the strength of surface plasmon resonance,[31] is also expected to be low due to the polycrystallinity of Ag/Au film prepared via electroless-deposition.[32] Similarly, hydrophobic Teflon film randomly deposited with Ag nanoparticle aggregates can also attain rhodamine 6G detection at femtomolar level.[5] However, the aggregated Ag nanoparticles may potentially suffer a structural and SERS signal reproducibility issue. Hence, an ideal superhydrophobic SERS platform is preferably built directly using plasmonic nanocrystals that support strong surface plasmon resonance(high Q-factor) for maximum SERS enhancement.[33]

Here, we demonstrate the fabrication of superhydrophobic Ag nanocube SERS platform and its suitability for highly diluted, small volume analyte detection. Our strategy emphasizes the synergy between the intense electromagnetic field confinement brought about by single crystalline Ag nanocubes and superhydrophobic surfaces with analyte concentrating effect to achieve ultrasensitive trace molecular detection using SERS. Controlled assembly of Ag nanocubes by the Langmuir-Blodgett technique is conducted to create surfaces with large-area plasmonic hotspots as well as generate optimal surface roughness for superhydrophobicity. An additional thin Ag coating is evaporated over the Ag nanocubes to improve the stability of the Ag nanocube array against nanoparticle dispersion upon addition of analyte droplet for SERS measurements. Finally, a chemical modification step of the surface with perfluorodecanethiol is performed to achieve superhydrophobicity. The superhydrophobicity of our Ag nanocube platforms at various surface densities is examined. We will quantitatively demonstrate that the analyte-concentrating effect, SERS detection limit, and analytical enhancement factor of our superhydrophobic Ag nanocube platform are superior to the hydrophilic Ag surface. Our protocol is a general method that provides a simple, cost-effective approach to develop a stable and uniform superhydrophobic SERS platform for trace molecular sensing.

RESULTS AND DISCUSSION

Single crystalline Ag nanocubes are used as the building blocks for our superhydrophobic SERS sensing platform. Ag nanocubes exhibit strong and distinct localized surface plasmon resonances across the visible spectrum owing to their excellent monodispersity, single crystallinity, and multiple sharp edges that can serve as plasmonic hotspots where electromagnetic fields are strongly localized.[31] Ag nanocubes are synthesized by the polyol method using 1,5-pentanediol as both the solvent and reducing agent, poly(vinylpyrrolidone) as the capping agent, and silver nitrate as the precursor.[34] The size distribution of Ag nanocubes is 102 ± 9 nm (Figure S1, Supporting Information). These Ag nanocubes are synthesized in large quantities, making them ideal building blocks for a large-scale solution-based fabrication technique to generate nanoscale roughness necessary for superhydrophobicity.

Surface roughness and chemical functionality are two key factors in achieving superhydrophobicity for our plasmonic nanocrystal platform. Surface roughness is created by assembling amphiphilic poly(vinylpyrrolidone)-capped Ag nanocubes into 2D arrays using the Langmuir-Blodgett technique,[35] a versatile technique to derive long-range order and uniform monolayer of nanocubes. In addition, the variation of surface pressure during Langmuir-Blodgett assembly can be employed to control the surface density of the nanoparticles and compactness of monolayer, which are directly correlated to the surface roughness of a substrate (Figure 1A).

The surface density of the the Ag nanocube array is monitored by the surface pressure (Π)—area isotherm during Langmuir-Blodgett assembly (Figure 1B). Upon compression, the color of the Ag nanocube monolayer suspended at the water−air interface transforms from yellow green (at Π = 8 mN m^{-1}) to brownish green (at Π = 10 mN m^{-1}) and eventually to metallic silver color (at Π = 18 mN m^{-1}), as observed from the digital images of Figure 1B. The changes in reflection color arise from the changes in plasmonic response due to coupling between adjacent nanocubes during the assembly.[36] At 3 < Π < 12 mN m^{-1}, the nanocubes are sparsely and randomly oriented (Figure 1C−F), denoting a two-dimensional liquid−gas transition phase.[37] From Π > 12 mN m^{-1} onwards, a denser nanocube assembly is achieved (Figure 1G, H), equivalent to a liquid phase of Ag which is typically characterized by the exponential increase of surface pressures with decreasing surface area. The increase in compactness of Ag nanocube monolayer can be further illustrated using particle density, in which the particle concentration increases gradually from 11 to 57 to 79 particles/μm^2 at surface pressures of 3, 10, and 18 mN m^{-1}, respectively.

The root-mean-square (rms) surface roughness of Ag nanocube array is then quantified using atomic force microscopy (AFM) as a direct parameter for the asperities effect on hydrophobicity (detailed discussion of rms roughness in Figure S2, Supporting Information). We have chosen nanocubes assembled using surface pressures ranging from 3, 6, 8, 10, 13, 15, and 18 mN m^{-1} for the surface roughness investigation. The nanocubes assembled at gas phase, Π < 3 mN m^{-1}, are not explored because the packing is deemed too scattered to achieve a rough Ag nanocube monolayer for superhydrophobicity. From the AFM characterization, we observe that the variation in surface roughness of the nanocube array does not scale linearly with the increase in surface pressures (Figure 1I). Initially, as surface pressure increases from 3 to 6 mN m^{-1}, the corresponding surface roughness of the substrates increases from 36 to 40 nm. However, further increase in surface pressure from 6 to 18 mN m^{-1} during the assembly leads to a decrease in surface roughness from 40 to 11 nm instead. This is because increasing surface pressure reduces the interparticle spacing, making the nanocube array more compact and results in an overall decrease of surface roughness instead (detailed discussion in Scheme S1, Supporting Information). Note that the AFM measurements may underestimate the surface roughness of the Ag nanocube array at higher surface densities because the AFM tip may not be able to probe through the well-packed Ag nanocube layer. Nevertheless, an optimal surface roughness of 40 nm is achieved by assembling nanocubes at surface pressure of 6 mN m^{-1} during the Langmuir-Blodgett process. From here onwards, Ag nanocube arrays of 40 nm surface roughness are used for further analysis, unless otherwise stated. This is to ensure that optimal surface roughness can be achieved for maximum amplification of surface hydrophobicity.

We then functionalize the Ag nanocube array with 1*H*,1*H*,2*H*,2*H*-perfluorodecanethiol to impart chemical-induced hydrophobicity to the surface. When the Ag nanocube array is directly functionalized with perfluorodecanethiol (Figure 2A-(i)), the as-prepared Ag nanocube array cannot support a stable water droplet. Upon water droplet addition,

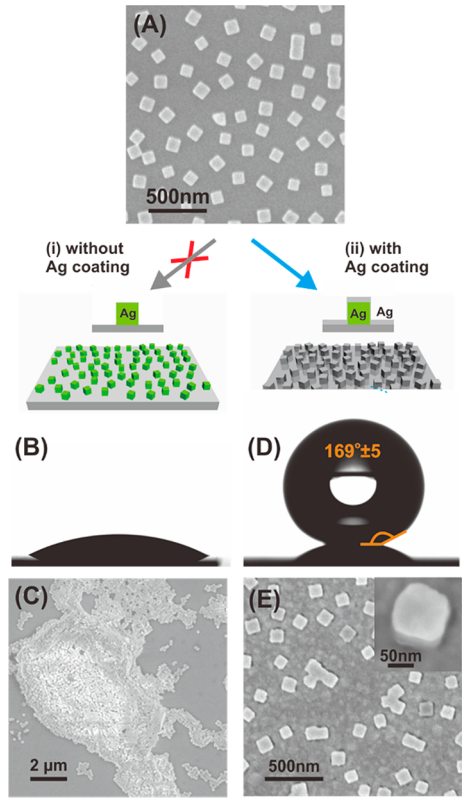

Figure 2. Comparison between the stability of uncoated and coated Ag nanocube array. (A) SEM image of uncoated Ag nanocube array. (B) A collapsed droplet when the uncoated Ag nanocube array redispersed. (C) SEM image of the uncoated Ag nanocube array after the water droplet is dried. (D) High advancing water contact angle on coated Ag nanocube array, illustrating its stability against redispersal. (E) SEM image of the coated Ag nanocube array. Inset is the SEM image of the tilted substrate to depict the "welding" of Ag nanocubes to the silicon surface by the additional Ag coating.

the water droplet collapses and a contact angle of less than 20° is attained in a matter of seconds (Figure 2B). In addition, the water droplet becomes silverish in color (Figure S3A, B, Supporting Information). SEM imaging of the Ag nanocube array after the water droplet addition (Figure 2C) indicates that Ag nanocubes have redispersed into the water droplet and formed aggregates upon drying. The long-range order of the entire Ag nanocube monolayer is disrupted, indicating a lack of adhesion of Ag nanocubes to the silicon substrate. Hence, the as-assembled perfluorodecanethiol-functionalized Ag nanocube monolayer is unstable and unsuitable for long-term SERS sensing applications.

To enhance the stability of the Ag nanocube array, we evaporate an additional intermediate adhesive layer of 2 nm Cr and subsequent 25 nm Ag coating to improve adhesion of Ag nanocubes to silicon substrate (Figure 2A-(ii)). The Ag coating is chosen at 25 nm to provide sufficient thickness to "weld" the edges to the silicon substrate for improved stability. Thinner Ag coatings were also attempted, but this did not reduce the instability of the Ag nanocube array. The coated Ag nanocube array is subsequently chemically functionalized with perfluorodecanethiol to impart hydrophobicity. SEM imaging in Figure 2E indicates Ag coating is homogeneously deposited on both the Ag nanocubes and silicon surfaces. The morphology of nanocubes is well preserved, with the bottom edges of the Ag nanocubes "welded" to the silicon surface by the additional Ag coating, and the sides of Ag nanocubes appear to have a relatively thinner coating compared to the top due to the unidirectional isotropic deposition intrinsic for the thermal evaporation method (inset of Figure 2E). AFM measurements indicate negligible change in surface roughness before and after Ag coating (Figures S4 and S5, Supporting Information). The Ag deposited Ag nanocube array is very stable during the contact angle measurement. An advancing contact angle of 169° ± 5° is measured after chemical modification of the substrate with perfluorodecanethiol, indicating superhydrophobicity of the substrate has been achieved (Figure 2D). This additional Ag coating not only enhances the stability of the nanocube monolayer but also improves the hydrophobicity of the substrate by masking the hydrophilic silicon surface. With the ability to impart stability and superhydrophobicity without significant deformation to the underlying Ag nanocubes, the evaporation of an additional Ag coating is clearly a better method to solve the redispersal issue compared to other chemical and physical methods attempted (discussed in detail in Figure S6, Supporting Information).

The superior water-repelling property of our superhydrophobic Ag nanocube substrate is demonstrated by studying its interaction with an approaching sessile droplet of water. Figure 3A-(i) indicates that only a very small solid–liquid contact area is observed. In contrast, for non-superhydrophobic surface (prepared at Π = 18 mN m^{-1}, Figure 3A-(ii)), a sessile water droplet readily adheres to the surface and results in the spreading of water droplet over a much wider surface area. These observations demonstrate that our superhydrophobic surface repels water, ensuring minimal interaction with water droplet.

Advancing contact angle of the coated Ag nanocube array, which also denotes the maximum contact angle achievable, is plotted against its surface roughness to study the relationship between hydrophobicity and roughness (Figure 3B). When the surface roughness of coated Ag nanocube array is in the range of 10–20 nm, the advancing contact angles are in the range of

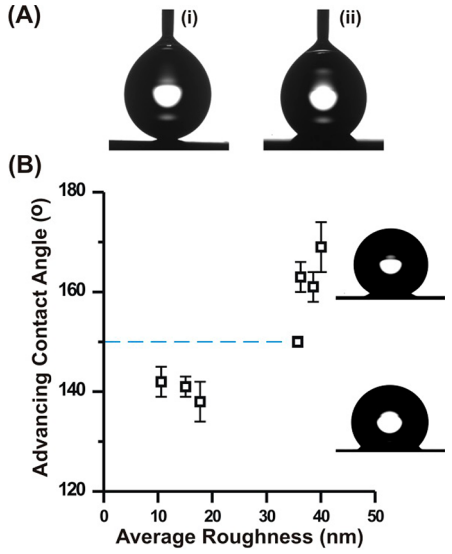

Figure 3. Illustration of the water-repelling effect of superhydrophobic substrate and the relationship between surface roughness and hydrophobicity (advancing contact angle). (A) Sessile water droplet placed in close proximity to a (i) superhydrophobic (prepared at Π = 6 mN m^{-1}) and (ii) nonsuperhydrophobic surface (prepared at Π = 18 mN m^{-1}). (B) Plot of advancing contact angle as a function of average surface roughness.

140° ± 4°. As the surface roughness further increases to 35–40 nm, superhydrophobicity is achieved, with a maximum advancing contact angle of 169° ± 5° attained. In contrast, superhydrophobicity cannot be achieved without the aid of roughness created by the Ag nanocubes. A flat evaporated Ag film functionalized with perfluorodecanethiol with negligible surface roughness has an advancing contact angle of 77° ± 3° (Figure S7, Supporting Information). Similarly, chemical functionality is also essential in imparting superhydrophobicity; an as-prepared coated Ag nanocube array with 40 nm surface roughness that is not functionalized with perfluorodecanethiol exhibits an advancing contact angle of 131° ± 2°, still 20° shy of superhydrophobicity. A detailed discussion is presented in the Supporting Information (Figure S7) using different ligand molecules, and the results demonstrate that both the surface roughness and chemical functionality are crucial in attaining superhydrophobic state, which agrees well with the theoretical Wenzel model[38] and Cassie-Baxter model of superhydrophobicity.[39]

Contact angle hysteresis, defined as the difference between advancing and receding contact angles, is a measure of the water adhesion (pinning) onto our substrates, a crucial examination of liquid analyte concentrating effect for the subsequent SERS measurements. Generally, a larger contact angle hysteresis indicates a stronger adhesion/pinning of water to the surface. The contact angle hysteresis of all coated Ag nanocube arrays ranges from 46° to 73° (Table S1, Supporting Information). This indicates that our Ag nanocube arrays have an intermediate adhesion property in between that of lotus-like surfaces (<10°) and rose-petal-like surfaces (>90°). Such intermediate adhesion is commonly found on surfaces with only primary nanoscale surface roughness.[19]

The extinction spectra of Ag nanocube solution, as-prepared Ag nanocube array, and Ag deposited Ag nanocube array are compared in Figure 4. The aim is to verify the localized surface plasmon resonance (LSPR) modes of the coated Ag nanocube

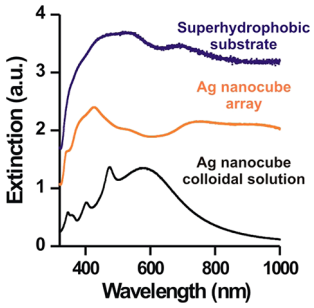

Figure 4. Localized surface plasmon resonance (LSPR) at different stages of protocol. The plot shows the extinction spectra of Ag nanocube colloidal solution (black), Ag nanocube array (orange), and superhydrophobic surface (blue) coated with 2 nm Cr and 25 nm Ag. Both Ag nanocube array and superhydrophobic surface are prepared on quartz using Langmuir-Blodgett surface pressure of 6 mN m^{-1}.

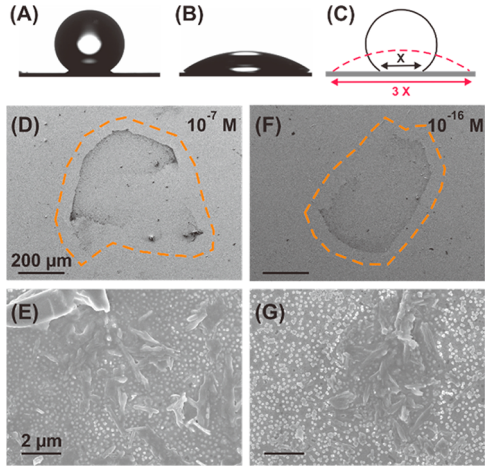

Figure 5. Concentrating effect on the superhydrophobic surface. Static contact angle images of (A) superhydrophobic substrate and (B) hydrophilic surface. (C) Schematic depicting maximum contact area on the superhydrophobic surface and hydrophilic surface. SEM images of the effective spot area and illustration of the aggregates within the spot at (D, E) 10^{-7} M and (F, G) 10^{-16} M.

array for subsequent SERS application. For colloidal Ag nanocube solution, the localized surface plasmon resonances at 346, 403, 475, and 580 nm can be assigned to octupole (346 nm), quadrupole (403 nm and 475 nm), and dipole resonances (580 nm), respectively.[40] For the as-prepared Ag nanocube array and superhydrophobic substrate, broadening of localized surface plasmon resonance spectrum is clearly illustrated between wavelengths of 350 and 1000 nm. This can be attributed to the plasmonic coupling between neighboring Ag nanocubes and Ag nanocubes with evaporated Ag coating, respectively.[36,41−44] It is noted that the extinction of the superhydrophobic SERS substrate is slightly noisier compared to the others. The origin of the noise for superhydrophobic SERS substrate could potentially be attributed to the increased opaqueness that reduces the optical transmission when an additional 25 nm Ag is evaporated onto the Ag nanocube array (Π = 6 mN m^{-1}). As optical transmission is decreased, the signal collected by the detector is also reduced, making the spectrum noisy due to increased sensitivity to external factors such as fluctuation of power intensity.

To demonstrate the liquid analyte concentrating effect of our superhydrophobic SERS platform in enhancing the SERS detection limit, we perform a droplet-size analysis on a superhydrophobic Ag nanocube array and a hydrophilic O_2-plasma-treated silicon substrate, each with static contact angles of 155° ± 2° and 36° ± 5°, respectively. Static contact angle, a result of the equilibrium between a static sessile drop and the surface, is discussed instead of advancing contact angle as latter SERS application involves the use of static analyte droplet. When 1-μL rhodamine 6G-containing water droplets are dispensed on both surfaces, the maximum solid−liquid contact area on the superhydrophobic surface is 0.50 mm^2, 9-fold smaller than the 4.5 mm^2 spot area of the hydrophilic surface (Figure 5A−C). The calculated ratio illustrates that a liquid/analyte concentration factor of ∼9 can be achieved using our superhydrophobic SERS substrate relative to a hydrophilic surface. That is, an equimolar and equal volume of analyte solution deposited on the superhydrophobic surface will be nine times more concentrated than on the hydrophilic substrate.

On the other hand, upon drying 1 μL of 10^{-7} and 10^{-16} M droplets of rhodamine 6G molecules on our superhydrophobic surfaces, spot sizes with a range of 0.32 ± 0.06 mm^2 (Figure 5D−G) are quantified. This is an analyte concentrating factor of 14 times as compared to a hydrophilic surface when in dry state. We notice that, when compared to its liquid state, a 1.6-fold reduction in rhodamine 6G surface area is observed in the dry state. The result again suggests that our superhydrophobic Ag nanocube platform exhibits intermediate Wenzel and Cassie-Baxter behavior. During the drying process, the droplet size shrinks to a smaller droplet area (an indication of Cassie-Baxter's lotus-like behavior) before being pinned (an indication of Wenzel's rose-petal-like behavior) to the as-measured dried surface area. These results demonstrate that our superhydrophobic surface is able to concentrate and direct liquid analyte into a small area to enhance detection sensitivity, which is essential for SERS detection of trace molecules.

We examine the SERS responses of our superhydrophobic Ag nanocube surfaces using rhodamine 6G so that a comparison can be made with the works of other groups.[6,27] Polarization effect on Ag nanocubes, as reported by a previous study,[45] will not be considered due to the various orientations of Ag nanocubes present in the close-packed array which, collectively, is not likely to exhibit polarization effect within the laser spot during SERS measurements. SERS spectra of various rhodamine 6G concentrations on the superhydrophobic SERS surface (Figure 6) show characteristic vibrational features at 610, 1092, 1177, 1375, and 1568 cm^{-1}, attributed to C−C−C in-plane bending, β(CH), CH in-plane bending, and two aromatic C−C stretching, respectively (Figure 6A).[6,46,47] Here, the intensity of the Raman band at 610 cm^{-1}, the vibration with the highest signal sensitivity, is selected for comparison across different analyte concentrations. A control analysis of the superhydrophobic SERS substrate in the absence of rhodamine 6G ("Control" in Figure 6B) gives a featureless SERS spectrum between 450 and 1800 cm^{-1}. Hence, the perfluorodecanethiol molecules have negligible contribution to the SERS signal within the Raman shift window of interest. This further illustrates that our protocol to fabricate superhydrophobic SERS substrate does not introduce Raman-interfering, non-analyte contaminants. This renders trace molecular sensing reliable.

Figure 6B depicts the magnified SERS spectra near the 610 cm^{-1} Raman shift window for 10^{-8} to 10^{-16} M rhodamine 6G concentrations (also in Figure S9, Supporting Information). At

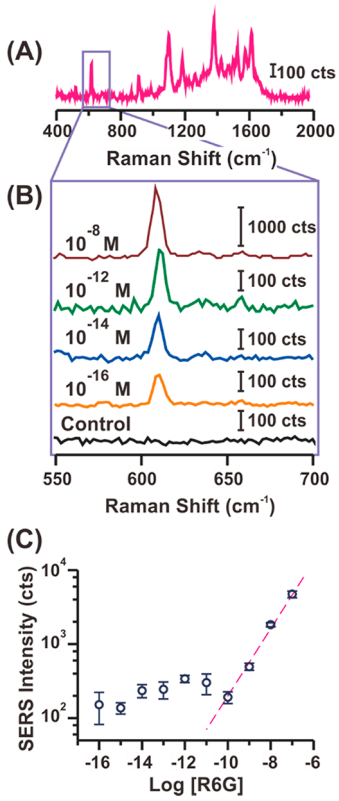

Figure 6. Application of superhydrophobic surface for trace analysis using rhodamine 6G as probe molecule. (A) SERS spectra of rhodamine 6G on superhydrophobic SERS substrate and (B) concentration ranging from 10^{-8} to 10^{-16} M. (C) SERS intensities at 610 cm^{-1} for rhodamine 6G concentration ranging from 10^{-7} to 10^{-16} M. Error bars were obtained with at least 6 repeated trials. Eye guided dot line indicates linear relationship of SERS intensity with analyte concentration up to 10^{-10} M. Control refers to SERS scan on superhydrophobic substrate in the absence of rhodamine 6G.

high rhodamine 6G concentration of 10^{-8} M, a SERS intensity of 1830 counts is obtained. A 10^4-fold dilution of rhodamine 6G to 10^{-12} M decreases the SERS intensity to ~341 counts. Decreasing the concentration of rhodamine 6G further to 10^{-16} M leads to a decrease of SERS intensity to 152 counts. At 10^{-16} M, signal-to-noise ratio of >3 and moderate reproducibility (discussed in detailed in Figure S10, Supporting Information) are still observed. Below 10^{-16} M, the signal-to-noise ratio is <3 and the Raman band is considered as indistinguishable from the background noise. Hence, the detection limit of our superhydrophobic SERS substrate is 10^{-16} M for rhodamine 6G. We would like to emphasize that prior to SERS analysis, the Ag-based superhydrophobic SERS substrates have been exposed to ambient conditions for at least one week for various characterization. Despite the susceptibility of Ag to oxidation, low detection limit is consistently achieved. The results affirm the sustainability and suitability of our substrates for detection of highly diluted samples (further discussion on sustainability upon prolonged storage in Figure S11, Supporting Information).

Quantitative comparison of the SERS intensities as a function of rhodamine 6G concentration demonstrates that a linear SERS response can be obtained over rhodamine 6G concentrations ranging from 10^{-10} to 10^{-7} M. This SERS response-concentration relationship is similar to literature on homogeneous SERS substrates,[2] indicating that our superhydrophobic SERS substrate can be applied for quantitative detection of analyte molecules in the 10^{-10}–10^{-7} M concentration window. An estimated extrapolation of SERS intensities towards analyte concentrations $<10^{-10}$ M (Figure 6C, dash lined guideline) estimates that SERS intensity at 610 cm^{-1} should fall below 100 counts in which it will no longer be distinguishable from the background. This estimation approximates the detection limit of the SERS substrate to be in the range of 10^{-10} to 10^{-11} M, shown by the linear portion of Figure 6C. Contrary to this theoretical estimation, we continue to observe SERS signals of ~100–300 counts in the concentration range of 10^{-11} to 10^{-16} M, with all SERS intensities exhibiting signal-to-noise ratio of >3. The physical adsorption of rhodamine 6G molecules on the superhydrophobic substrate can be approximated as a Langmuir isotherm.[6] Below 10^{-11} M, rhodamine 6G molecules are randomly deposited on the superhydrophobic substrate, forming submonolayer aggregates on the substrate (Scheme S2, Supporting Information). With decreasing concentrations, the occurrence of such aggregates decreases correspondingly. Consequently, SERS signals are collected from these isolated submonolayer aggregates over the concentration range of 10^{-11} to 10^{-16} M, leading to similar signal intensities observed despite large concentration changes. This result is a strong demonstration that the 14-fold analyte concentrating effect of our superhydrophobic Ag nanocube platforms can lower the detection limit of analyte molecules to 10^{-16} M (100 aM).

In contrast, no distinct rhodamine 6G Raman band is observed using evaporated Ag film, even when 10^{-7} M is used (Figure S8, Supporting Information). The general high background signal as observed can be attributed to the fluorescence of rhodamine 6G at the excitation wavelength of 532 nm. The absence of Raman band is due to the low Q factor plasmon resonance associated with the polycrystallinity of evaporated Ag film that causes weak surface plasmon polariton propagation. Note that direct comparison between the superhydrophobic Ag nanocube platform with its hydrophilic one is not possible owing to the nanocube redispersion issue associated with the hydrophilic Ag nanocube layer.

We also calculate the analytical enhancement factor (AEF) to quantify the SERS enhancement of analyte molecules adsorbed on the superhydrophobic SERS substrate.[48] Analytical EF is defined as: $AEF = [(I_{SERS})/(I_{Raman})] \times [(C_{Raman})/(C_{SERS})]$, where I_{SERS} and I_{Raman} are the signals recorded on SERS and normal Raman substrates at lowest concentration, whereas C_{SERS} and C_{Raman} are the corresponding concentrations measured using superhydrophobic Ag nanocube platform and normal Raman substrates, respectively. The analytical enhancement factor is calculated on the basis of the intensities of the 610 cm^{-1} band of rhodamine 6G on SERS and Raman spectra at concentrations of 10^{-16} and 10^{-4} M, respectively (Figure S12, Supporting Information). An analytical enhancement factor of 10^{11} has been achieved using our superhydrophobic SERS platform, illustrating that our superhydrophobic SERS substrate provides a 10^{11} enhancement of signal intensity compared to a hydrophilic normal Raman substrate.

In order to analyze the contribution of each factor to the high analytical enhancement factor (AEF) observed, we systematically compare the AEF of the substrates at different stages of our fabrication. The substrates include the superhydrophobic SERS substrate, thermally evaporated Ag film, coated Ag nanocube array prior to perfluorodecanethiol functionalization, and a superhydrophobic non-plasmonic active bead array

coated with an Ag film. In general, the static contact angles of all of the substrates are in the range of ~150°, except for the thermally evaporated Ag film and unfunctionalized coated Ag nanocube array which have static contact angles of 117° ± 1° and 106° ± 4°, respectively. As such, the contribution of concentrating effect arising from the superhydrophobicity of the substrates to the AEF is assumed to be the same. Also, the AEF is calculated on the basis of the detection limit of every individual substrate, which is defined as the lowest concentration of rhodamine 6G detectable with SERS intensities >100 and signal-to-noise ratio >3.

Firstly, the AEF of our superhydrophobic SERS substrate (Figure 7A) and Ag film (Figure 7B) is calculated to be 10^{11} and 10^{2}, respectively. This large increase of approximately 10^{9}-fold AEF on our superhydrophobic SERS substrate can potentially be attributed to several factors, including the concentrating effect (approximately 9-fold enhancement as discussed previously, Figure 5), increased amount of plasmonic Ag available as roughness increases, and more importantly, the presence of single crystalline Ag nanocubes. Furthermore, Ag nanocubes have been shown to bring about a greater local electromagnetic field enhancement as compared to nanospheres. This justifies the use of nanocubes in creating a superhydrophobic SERS substrate in our work.[49]

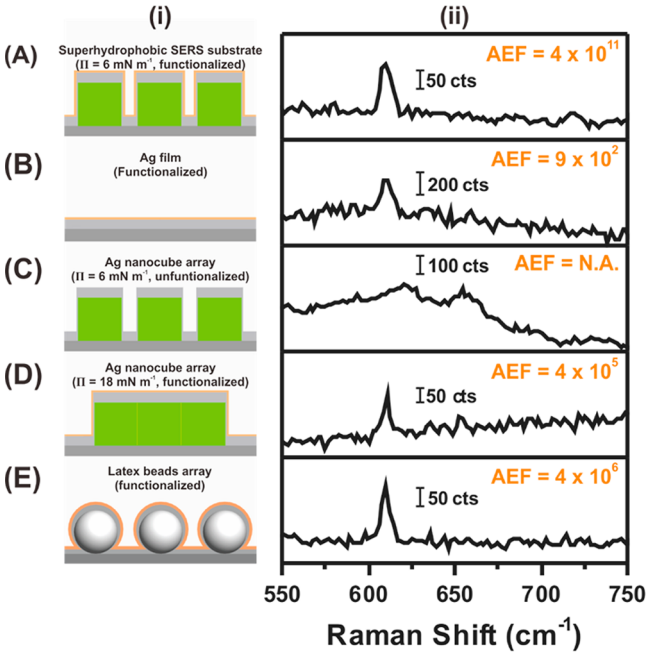

Figure 7. Comparison of analytical enhancement factor (AEF) of different substrates. (A) Superhydrophobic SERS substrate. (B) Perfluorodecanethiol-functionalized (brown) Ag film. (C) Unfunctionalized Ag nanocube array at Π = 6 mN m^{-1}. (D) Perfluorodecanethiol-functionalized Ag nanocube array at Π = 18 mN m^{-1}. (E) Superhydrophobic latex beads array. (i) Schematic illustration and (ii) SERS spectrum of respective type of substrate. AEF is calculated on the basis of the detection limit of individual substrates which is 10^{-16}, 10^{-7}, 10^{-10}, and 10^{-11} M for (A), (B), (D), and (E), respectively.

Next, we compare our superhydrophobic SERS substrate with a coated Ag nanocube array assembled at Π = 6 mN m^{-1} but not functionalized by perfluorodecanethiol (Figure 7C), with a static contact angle of 106° ± 4°. A broad background spectrum is observed near the 610 cm^{-1} region with the presence of characteristic peaks of poly(vinylpyrrolidone),[42] the capping agent used for Ag nanocube synthesis. Hence, the application of unfunctionalized Ag nanocube array, even at the same surface pressure, is unsuitable for trace detection due to the presence of interference from poly(vinylpyrrolidone). This experiment demonstrates the need for ligand functionalization with perfluorodecanethiol to both reduce signal interference and increase surface hydrophobicity, as established earlier.

We then compare the AEF of our superhydrophobic SERS substrate and a perfluorodecanethiol-functionalized, highly compact Ag nanocube array assembled at Π = 18 mN m^{-1} (Figure 7D). The calculated AEF are 10^{11} and 10^{5}, respectively. The lower AEF on the highly compact Ag nanocube array is rather counterintuitive, since the higher density of Ag nanocubes should give rise to higher SERS signals with more hotspots present. We attribute this phenomenon to the loss of electromagnetic enhancement, especially from the top of Ag nanocubes, as the separation between analyte molecules and Ag nanocubes increases when 25 nm Ag is evaporated on it. However, it should be emphasized again on the need of this 25 nm Ag to enhance the stability of the Ag nanocube array where thinner evaporated Ag layer is insufficient in stabilizing the Ag nanocubes. Also, we acknowledge the possibility of additional enhancement brought about by increased Ag coating in the superhydrophobic substrate with larger inter-nanocube spacing. Hence, we infer that stronger enhancement originates from the sides of Ag nanocube which has a much thinner coating compared to the top (in Figure 2E). Such unidirectional isotropic deposition is intrinsic for Ag thermal evaporation.

Finally, we compare the AEF of our superhydrophobic SERS substrate with a superhydrophobic substrate (static contact angle = 149° ± 3°) fabricated using non-plasmonic active beads (Figures 7E and S13, Supporting Information). The AEF is calculated to be 10^{6} for the non-plasmonic active beads. By comparing these two substrates, we minimize differences arising from the concentrating effect and amount of evaporated Ag layer. Thus, the additional 10^{5}-fold enhancement in our superhydrophobic SERS substrate is attributed to the presence of hotspots on and between the Ag nanocubes and the need of plasmonic nanocrystals as the building blocks is clearly evident.

With the breakdown of the AEF contribution of different features in our superhydrophobic SERS substrate, the high analytical enhancement factor with ultralow detection limit can be attributed to three factors. Firstly, a large extent of SERS enhancement can be expected due to the large numbers of hotspots generated from single crystalline Ag nanocubes with numerous sharp edges and corners. We also note the possibility of cube/cube and cube/evaporated-Ag plasmonic coupling to increase spatial electromagnetic enhancement through collective plasmonic effects in all *x*, *y*, and *z* planes.[11] Secondly, superhydrophobicity of the substrate minimizes solid−liquid contact area such that trace amount of analytes are concentrated/aggregated into a very small area to increase the analyte-to-signal ratio and, hence, improves detection sensitivity. Thirdly, the resonance of rhodamine 6G at excitation wavelength of 532 nm can also contribute to the partial enhancement of SERS signal.[46,50]

The incorporation of large-area plasmonic hotspots with a superhydrophobic surface as an analyte concentrator enables trace detection of rhodamine 6G at 10^{-16} M. The apparent detection limit is slightly inferior compared to the reported superhydrophobic surface prepared by lithography,[27] possibly due to the higher number of analyte molecules available as a

result of larger sample volumes (20 μL) used in the latter study. However, our superhydrophobic SERS platform excels in the case of limited sample availability, as only 1 μL of highly diluted sample is required for trace detection.

Our superhydrophobic SERS platform protocol possesses the advantage of rendering superhydrophobicity to plasmonic nanostructures directly. This minimizes overlapping of Raman signal from non-analyte molecules, such as the polymer matrix commonly used for superhydrophobic platforms that may interfere with SERS application, especially for trace molecular detection. Noting the distribution of individual Ag nanocubes is spaced out (spacing >50 nm) over the entire platform, the SERS enhancement can be mainly attributed to the sharp edges of the Ag nanocubes that generate strong and intense localized electromagnetic fields, giving rise to strong SERS sensing. In addition to trace and quantitative SERS analysis, our superhydrophobic SERS substrate exhibits other characteristics that enhance its appeal as a SERS substrate. Firstly, macroscopic properties, such as surface roughness and static and dynamic contact angles, are not significantly affected (relative standard deviations <20%) by nanoscopic inhomogeneity caused by partial randomization of the Ag nanocube arrays. Together with the stability enforced against redispersal, it is evident that our superhydrophobic SERS substrate possesses consistent and representative macroscopic properties for it to function as a uniform analytical platform for trace and quantitative analysis. Secondly, its intermediate adhesion behavior allows pinning of each droplet to a designated small area on the surface. This allows easy manipulation during analysis as well as enables simultaneous loading of different analyte solutions onto a single substrate, thus reducing the need for multiple superhydrophobic SERS substrates. Our protocol is also cost- and time-effective as equipment and procedures required are simple and low-cost.

CONCLUSIONS

We have demonstrated a cost- and time-effective fabrication of a superhydrophobic Ag nanocube platform that is capable of trace molecular sensing down to 10^{-16} M of rhodamine 6G. Quantitative analysis of analytes can also be achieved within a concentration window of 10^{-7} to 10^{-10} M. Importantly, only 1 μL of such highly diluted analyte solution is required, demonstrating its potential as a highly diluted, small volume analytical platform. With superhydrophobicity to enhance detection sensitivity such that only small sample volume is required for detection, our superhydrophobic SERS substrate can also be miniaturized to find potential application as an analytical platform in a lab-on-chip system. Furthermore, our strategy to render superhydrophobicity on plasmonic nanocrystals is general and can be extended to other nanoparticles to further improve SERS enhancement by tailoring the plasmonic interactions between the nanoparticles. This will open up an opportunity for the use of superhydrophobic SERS substrates towards trace toxin and/or molecule(s) detection in various fields ranging from industrial and environmental safety to criminology.

EXPERIMENTAL DETAILS

Chemicals. Silver nitrate (≥99%), anhydrous 1,5-pentanediol (PD, ≥97%), poly(vinylpyrrolidone) (PVP, average MW = 55 000 g/mol), 1*H*,1*H*,2*H*,2*H*-perfluorodecanethiol (PFDT, ≥97%), 1-dodecanethiol (DDT, ≥98%), rhodamine 6G (R6G, dye content ~95%), and latex beads (polystyrene, 0.1 μm mean particle size) were purchased from Sigma Aldrich; copper(II) chloride (≥98%) and 3-aminopropyltriethoxysilane (98%) were from Alfa Aesar. Ethanol (ACS, ISO, Reag. Ph Eur) was from EMSURE; *n*-hexane (AR, ≥95%) was obtained from RCI Labscan. All chemicals were used without further purification. Milli-Q water (>18.0 MΩ·cm) was purified with a Sartorius Arium 611 UV ultrapure water system.

Synthesis and Purification of Ag Nanocubes. The preparation of Ag nanocubes was carried out following the method described in the literature.[27] Briefly, 10 mL of $CuCl_2$ (8 mg/mL), PVP (20 mg/mL), and $AgNO_3$ (20 mg/mL) was separately dissolved in PD. The chemicals were sonicated and vortexed repeatedly to dissolve them. A 35 μL $CuCl_2$ solution was then added to the $AgNO_3$ solution. Then, 20 mL of PD in a 100 mL round bottomed flask was heated to 190° C for 10 min. A 250 μL PVP precursor was added to the flask dropwise every 30 s while 500 μL of $AgNO_3$ precursor was injected every min using a quick addition. The addition process continued until the greenish coloration of the reaction mixture faded off.

For the purification of Ag nanocubes, PD was first removed from the mixture through centrifugation. The Ag nanocube solution was then dispersed in 10 mL of ethanol and 100 mL of aqueous PVP solution (0.2 g/L). The resulting solution was vacuum filtered using PVDF filter membranes with pore sizes ranging from 5000, 650, 450, and 220 nm, repeated several times for each pore size. SEM imaging was performed from which the edge lengths of 100 Ag nanocubes are measured and analyzed using ImageJ software. The as-synthesized nanocubes were found to be obtained in high yield.

Preparation of Superhydrophobic Ag Nanocube Array. Si (100) substrates were cleaned prior to assembly of Ag nanocubes using oxygen plasma (FEMTO SCIENCE, CUTE-MP/R, 100W) for 5 min. The surface pressure was zeroed before the addition of PVP-capped Ag nanocubes; 800 μL of purified Ag nanocubes solution was dispersed in 1200 μL of chloroform and then spread over the water surface of the Langmuir-Blodgett (LB) trough (KSV NIMA, KN1002). The movement of the mechanical barrier of the Langmuir-Blodgett machine over the trough controls the surface pressure. Assemblies at various target surface pressures of 3, 6, 8, 10, 13, 15, and 18 mN m^{-1} were performed. Both the pull rate and compression rate were fixed at 2 mm s^{-1}. Cr and Ag films were deposited using a home-built thermal evaporator deposition system. A 2-nm Cr adhesion layer was first deposited, followed by a 25-nm Ag film to promote the adhesion of Ag nanoparticles onto silicon substrate. The deposition rates of Cr and Ag were 0.1 and 0.5 Å/s, respectively. The deposited rate was monitored in situ by a quartz crystal microbalance. Ag target with 99.99% purity was purchased from Advent Research Materials, UK. The coated Ag nanocube array was then functionalized by immersion into a 5 mM 1*H*,1*H*,2*H*,2*H*-perfluorodecanethiol in 1:1 ethanol/hexane solution for at least 15 h. For 1-dodecanethiol functionalization, the same steps were performed but in ethanolic solution instead.

Preparation of Latex Bead Array. Amine-terminated silicon substrates were prepared according to the literature prior to the dip-coating assembly.[51] Briefly, Si substrates were subjected to oxygen plasma treatment (FEMTO SCIENCE, CUTE-MP/R, 100W) for 15 min and subsequently immersed in 3-aminopropyltriethoxysilane/toluene solution (2 % by volume) for 60 min. Then, the amine-terminated Si substrates were rinsed with copious amounts of toluene, methanol, and ultrapure water. The amine-terminated substrates were immersed in an aqueous suspension of latex beads (1 %) for 10 min, removed, and blow dried with a stream of nitrogen. The latex bead array was later coated with 2-nm Cr and 25-nm Ag and subsequently functionalized with 1*H*,1*H*,2*H*,2*H*-perfluorodecanethiol using the same procedures described in Preparation of Superhydrophobic Ag Nanocube Array.

Analysis of R6G on As-Prepared SERS Substrate. R6G (4.79 mg/mL, 10^{-2} M) was prepared in aqueous solution using ultrapure water. Serial dilutions were performed to give a series of concentrations, ranging from 10^{-7} to 10^{-16} M; 1 μL droplets of each R6G concentration were placed on different locations of the superhydrophobic substrate. The droplets were allowed to dry under ambient condition before proceeding with SERS characterization.

Materials Characterization. SEM imaging was performed using a JEOL-JSM-7600F microscope. UV-vis spectroscopic measurements were conducted with a Cary 60 UV-Vis spectrometer. The roughnesses of the sample before and after the coating were measured using JPK Nanowizard3 BioScience atomic force microscopy (AFM) on a Zeiss inverted microscope. Silicon cantilevers from Budgetsensors (model Tap300-G with 30 nm Aluminum back reflex coating) were used for AC mode (non-contact mode) operation. Contact angles were measured on a Theta Lite tensiometer equipped with a Firewire digital camera. Static contact angles were measured with a 4 μL ultrapure water droplet. Advancing and receding contact angles were determined using drop shape analysis routine of a growing and shrinking drop of water, respectively. Each type of contact angle was performed at least five times across each substrate. SERS measurements were performed with at least six repeated trials using an *xy*-imaging mode of the Laser Raman Microscope RAMANtouch system with an excitation wavelength of 532 nm (power = 64.6 μW). A 20× objective lens with 10 s accumulation time was used between 450 and 1800 cm^{-1}.

■ ASSOCIATED CONTENT

Ⓢ Supporting Information

Details of various characterization, Raman controls, and additional discussion. This information is available free of charge via the Internet at http://pubs.acs.org/.

■ AUTHOR INFORMATION

Corresponding Author

*E-mail: xyling@ntu.edu.sg.

Notes

The authors declare no competing financial interest.

■ ACKNOWLEDGMENTS

X.Y.L., Y.H.L., and Y.C. thank the support from National Research Foundation, Singapore (NRF-NRFF2012-04), and Nanyang Technological University's start-up grant.

■ REFERENCES

(1) Qian, X. M.; Nie, S. M. *Chem. Soc. Rev.* **2008**, *37*, 912−920.
(2) Mulvihill, M.; Tao, A.; Benjauthrit, K.; Arnold, J.; Yang, P. *Angew. Chem., Int. Ed.* **2008**, *47*, 6456−6460.
(3) Kim, A.; Barcelo, S. J.; Williams, R. S.; Li, Z. *Anal. Chem.* **2012**, *84*, 9303−9309.
(4) Boyd, S.; Bertino, M. F.; Ye, D. X.; White, L. S.; Seashols, S. J. *J. Forensic Sci.* **2013**, *58*, 753−756.
(5) Shao, M.-W.; Lu, L.; Wang, H.; Wang, S.; Zhang, M.-L.; Ma, D.-D.-D.; Lee, S.-T. *Chem. Commun.* **2008**, 2310−2312.
(6) Lu, L.-Q.; Zheng, Y.; Qu, W.-G.; Yu, H.-Q.; Xu, A.-W. *J. Mater. Chem.* **2012**, *22*, 20986−20990.
(7) Ko, H.; Singamaneni, S.; Tsukruk, V. V. *Small* **2008**, *4*, 1576−1599.
(8) Blatchford, C. G.; Campbell, J. R.; Creighton, J. A. *Surf. Sci.* **1982**, *120*, 435−455.
(9) McLellan, J. M.; Siekkinen, A.; Chen, J.; Xia, Y. *Chem. Phys. Lett.* **2006**, *427*, 122−126.
(10) Sturman, B.; Podivilov, E.; Gorkunov, M. *Europhys. Lett.* **2013**, *101*, 57009.
(11) Chen, M.; Phang, I. Y.; Lee, M. R.; Yang, J. K. W.; Ling, X. Y. *Langmuir* **2013**, *29*, 7061−7069.
(12) Goh, M. S.; Lee, Y. H.; Pedireddy, S.; Phang, I. Y.; Tjiu, W. W.; Tan, J. M. R.; Ling, X. Y. *Langmuir* **2012**, *28*, 14441−14449.
(13) Hu, J.; Zhao, B.; Xu, W.; Fan, Y.; Li, B.; Ozaki, Y. *Langmuir* **2002**, *18*, 6839−6844.
(14) Saito, Y.; Wang, J. J.; Smith, D. A.; Batchelder, D. N. *Langmuir* **2002**, *18*, 2959−2961.
(15) Pazos-Perez, N.; Wagner, C. S.; Romo-Herrera, J. M.; Liz-Marzan, L. M.; de Abajo, F. J. G.; Wittemann, A.; Fery, A.; Alvarez-Puebla, R. A. *Angew. Chem., Int. Ed.* **2012**, *51*, 12688−12693.
(16) Barthlott, W.; Neinhuis, C. *Planta* **1997**, *202*, 1−8.
(17) Neinhuis, C.; Barthlott, W. *Ann. Bot.* **1997**, *79*, 667−677.
(18) Liu, K.; Yao, X.; Jiang, L. *Chem. Soc. Rev.* **2010**, *39*, 3240−3255.
(19) Teisala, H.; Tuominen, M.; Kuusipalo, J. *J. Nanomater.* **2011**, *2011*, 818707.
(20) Xue, Z. X.; Wang, S. T.; Lin, L.; Chen, L.; Liu, M. J.; Feng, L.; Jiang, L. *Adv. Mater.* **2011**, *23*, 4270−4273.
(21) Bhushan, B. In *Biomimetics*; Springer: Berlin Heidelberg: 2012; p 189−206.
(22) Feng, L.; Li, S.; Li, Y.; Li, H.; Zhang, L.; Zhai, J.; Song, Y.; Liu, B.; Jiang, L.; Zhu, D. *Adv. Mater.* **2002**, *14*, 1857−1860.
(23) Guo, Z.; Liu, W.; Su, B.-L. *J. Colloid Interface Sci.* **2011**, *353*, 335−355.
(24) Ling, X. Y.; Phang, I. Y.; Vancso, G. J.; Huskens, J.; Reinhoudt, D. N. *Langmuir* **2009**, *25*, 3260−3263.
(25) Shirtcliffe, N. J.; McHale, G.; Atherton, S.; Newton, M. I. *Adv. Colloid Interface Sci.* **2010**, *161*, 124−138.
(26) Xu, F.; Zhang, Y.; Sun, Y.; Shi, Y.; Wen, Z.; Li, Z. *J. Phys. Chem. C* **2011**, *115*, 9977−9983.
(27) De Angelis, F.; Gentile, F.; Mecarini, F.; Das, G.; Moretti, M.; Candeloro, P.; Coluccio, M. L.; Cojoc, G.; Accardo, A.; Liberale, C.; Zaccaria, R. P.; Perozziello, G.; Tirinato, L.; Toma, A.; Cuda, G.; Cingolani, R.; Di Fabrizio, E. *Nat. Photonics* **2011**, *5*, 682−687.
(28) Gentile, F.; Coluccio, M. L.; Coppede, N.; Mecarini, F.; Das, G.; Liberale, C.; Tirinato, L.; Leoncini, M.; Perozziello, G.; Candeloro, P.; De Angelis, F.; Di Fabrizio, E. *ACS Appl. Mater. Interfaces* **2012**, *4*, 3213−3224.
(29) Xu, B. B.; Zhang, Y. L.; Zhang, W. Y.; Liu, X. Q.; Wang, J. N.; Zhang, X. L.; Zhang, D. D.; Jiang, H. B.; Zhang, R.; Sun, H. B. *Adv. Opt. Mater.* **2013**, *1*, 56−60.
(30) Kahraman, M.; Balz, B. N.; Wachsmann-Hogiu, S. *Analyst* **2013**, *138*, 2906−2913.
(31) Rycenga, M.; Cobley, C. M.; Zeng, J.; Li, W.; Moran, C. H.; Zhang, Q.; Qin, D.; Xia, Y. *Chem. Rev.* **2011**, *111*, 3669−3712.
(32) Novotny, L.; van Hulst, N. *Nat. Photonics* **2011**, *5*, 83−90.
(33) Henzie, J.; Andrews, S. C.; Ling, X. Y.; Li, Z. Y.; Yang, P. D. *Proc. Natl. Acad. Sci. U.S.A.* **2013**, *110*, 6640−6645.
(34) Tao, A. R.; Ceperley, D. P.; Sinsermsuksakul, P.; Neureuther, A. R.; Yang, P. *Nano Lett.* **2008**, *8*, 4033−4038.
(35) Lee, Y. H.; Lee, C. K.; Tan, B.; Rui Tan, J. M.; Phang, I. Y.; Ling, X. Y. *Nanoscale* **2013**, *5*, 6404−6412.
(36) Tao, A.; Sinsermsuksakul, P.; Yang, P. *Nat. Nanotechnol.* **2007**, *2*, 435−440.
(37) Petty, M. C. *Langmuir-Blodgett Films: An Introduction*; Cambridge University Press: Cambridge, 1996.
(38) Wenzel, R. N. *J. Phys. Colloid Chem.* **1949**, *53*, 1466−1467.
(39) Cassie, A. B. D. *Discuss. Faraday Soc.* **1948**, *3*, 11−16.
(40) Lee, Y. H.; Chen, H. J.; Xu, Q. H.; Wang, J. F. *J. Phys. Chem. C* **2011**, *115*, 7997−8004.
(41) Su, K. H.; Wei, Q. H.; Zhang, X.; Mock, J. J.; Smith, D. R.; Schultz, S. *Nano Lett.* **2003**, *3*, 1087−1090.
(42) Mahmoud, M. A.; Tabor, C. E.; El-Sayed, M. A. *J. Phys. Chem. C* **2009**, *113*, 5493−5501.
(43) Yang, Y.; Shi, J.; Tanaka, T.; Nogami, M. *Langmuir* **2007**, *23*, 12042−12047.
(44) Jiang, C.; Markutsya, S.; Tsukruk, V. V. *Langmuir* **2003**, *20*, 882−890.
(45) McLellan, J. M.; Li, Z.-Y.; Siekkinen, A. R.; Xia, Y. *Nano Lett.* **2007**, *7*, 1013−1017.
(46) Hildebrandt, P.; Stockburger, M. *J. Phys. Chem.* **1984**, *88*, 5935−5944.
(47) Huang, Z.; Meng, G.; Huang, Q.; Yang, Y.; Zhu, C.; Tang, C. *Adv. Mater.* **2010**, *22*, 4136−4139.
(48) Le Ru, E. C.; Blackie, E.; Meyer, M.; Etchegoin, P. G. *J. Phys. Chem. C* **2007**, *111*, 13794−13803.

(49) Harvey, C. E.; van Schrojenstein Lantman, E. M.; Mank, A. J. G.; Weckhuysen, B. M. *Chem. Commun.* **2012**, *48*, 1742−1744.
(50) Dieringer, J. A.; Wustholz, K. L.; Masiello, D. J.; Camden, J. P.; Kleinman, S. L.; Schatz, G. C.; Van Duyne, R. P. *J. Am. Chem. Soc.* **2008**, *131*, 849−854.
(51) Howarter, J. A.; Youngblood, J. P. *Langmuir* **2006**, *22*, 11142−11147.